2011

Syntheses, characterization, density functional theory calculations, and activity of tridentate SNS zinc pincer complexes

John R. Miecznikowski
Fairfield University, jmiecznikowski@fairfield.edu

Wayne Lo
Matthew A. Lynn
Brianne E. O'Loughlin
Amanda P. DiMarzio

See next page for additional authors

Syntheses, Characterization, Density Functional Theory Calculations, and Activity of Tridentate SNS Zinc Pincer Complexes

John R. Miecznikowski[a]*; Wayne Lo[b]; Matthew A. Lynn[c];
Brianne E. O'Loughlin[a]; Amanda P. DiMarzio[a]; Anthony M. Martinez[a];
Lorraine Lampe[a]; Kathleen M. Foley[a]; Lauren C. Keilich[a]; George P. Lisi[a]; Daniel J. Kwiecien[a]; Cristina M. Pires[a]; William J. Kelly[a], Nathan F. Kloczko[a], and Kaitlyn N. Morio[a]

[a]Department of Chemistry and Biochemistry, Fairfield University, 1073 North Benson Road, Fairfield, CT 06824. U.S.A.

[b] Department of Chemistry, Boston College, 140 Commonwealth Avenue, Chestnut Hill, MA 02467. U.S.A.

[c]Department of Science and Mathematics, National Technical Institute for the Deaf, Rochester Institute of Technology, 52 Lomb Memorial Drive, Rochester, NY 14623. U.S.A.

* Corresponding Author: Tel.: 1-(203) 254-4000 x 2125; Fax: 1-(203) 254-4034; Email: jmiecznikowski@fairfield.edu

Abstract:

A series of tridentate SNS ligand precursors were metallated with $ZnCl_2$ to give new tridentate SNS pincer zinc complexes. The zinc complexes serve as models for the zinc active site in Liver Alcohol Dehydrogenase (LADH) and were characterized with single crystal X-ray diffraction, ^{1}H, ^{13}C, and HSQC NMR spectroscopies and electrospray mass spectrometry. The bond lengths and bond angles of the zinc complexes correlate well to those in horse LADH. The zinc complexes feature SNS donor atoms and pseudotetrahedral geometry about the zinc center, as is seen for liver alcohol dehydrogenase. The SNS ligand precursors were characterized with ^{1}H, ^{13}C, and HSQC NMR spectroscopies and cyclic voltammetry, and were found to be redox active. Gaussian calculations were performed and agree quite well with the experimentally observed oxidation potential for the pincer ligand. The zinc complexes were screened for the reduction of electron poor aldehydes in the presence of a hydrogen donor, 1-benzyl-1,4-dihydronicotinamide (BNAH). The zinc complexes enhance the reduction of electron poor aldehydes. Density functional theory calculations were performed to better understand why the geometry about the zinc center is pseudo-tetrahedral rather than pseudo-square planar, which is seen for most pincer complexes. For the SNS tridentate pincer complexes, the data indicate that the pseudo-tetrahedral geometry was 43.8 kcal/mol more stable than the pseudo-square planar geometry. Density functional theory calculations were also performed on zinc complexes with monodentate ligands and the data indicate that the pseudo-tetrahedral geometry was 30.6 kcal/mol more stable than pseudo-square planar geometry. Overall, the relative stabilities of the pseudo-tetrahedral and pseudo-square planar systems are the same for this

coordination environment whether the ligand set is a single tridentate SNS system or is broken into three separate units. The preference of a d^{10} Zn center to attain a tetrahedral local environment trumps any stabilization gained by removal of constraints within the ligand set.

Keywords:

SNS pincer ligand
Mononuclear Zn complexes
X-ray crystallography
Cyclic voltammetry
Density functional theory calculations
Aldehyde reductions

1. Introduction:

Bioinorganic chemists have made contributions toward the understanding of enzymatic activity through the synthesis and subsequent structural and functional characterization of model complexes for metalloenzyme active sites [1]. Model complexes are low molecular mass systems that seek to mimic the metalloenzyme in terms of ligand donor atoms, structure, and oxidation states [2]. Bio-inspired model complexes can be prepared to investigate the structure and function of enzymes through the use of Nature as a model for the design of highly active and efficient catalysts.

Liver alcohol dehydrogenase (LADH) is a zinc metalloenzyme that catalyzes the oxidation of alcohols to aldehydes and ketones, and also catalyzes the reverse reaction: the reduction of a ketone or an aldehyde to an alcohol [1,3]. The crystal structure of horse LADH has been solved [4]. The resting enzyme has a zinc(II) metal center which is pseudo-tetrahedrally ligated with one N-histidine side chain, two S-cysteine side chains,

and one labile water molecule. The nitrogen and sulfur donor atoms are provided by histidine and cysteine residues of a single polypeptide chain [5]. Several structural models for LADH have been reported with the same donor atoms as the metalloenzyme [6-13]. In some cases, reactivity data was not reported [14]. Reactivity has also been reported for zinc LADH model complexes with donor atoms that are different than the enzyme's active site [15].

In our efforts to understand the catalytic activity of such a metalloenzyme, we have chosen to model the structure and reactivity of the zinc active site through the use of a new family of robust pincer ligands that provide the same S,N,S donor atoms as the enzyme. Tridentate pincer ligands, first published in 1976, offer several advantages as compared to monodentate ligands. First, their metallation is favored due to a less negative delta entropy of formation as compared to monodentate ligands, conferring added stability to their metal complexes [16]. Second, tridentate pincer ligands are known to inhibit dimerization, a process that could slow or inhibit catalytic activity. Third, the structural and electronic properties of the tridentate ligand can be systematically changed by the use of slightly different materials in their synthetic preparation. The tridentate pincer ligand usually coordinates to the metal in a meridional fashion. Sometimes both of the metallocycles pucker, leading to a pseudo-facial coordination mode.

Pincer ligands have been utilized successfully in organometallic chemistry to prepare highly catalytically active and robust complexes [17]. Interestingly, to the best of our knowledge, such ligand systems have not been used frequently in bio-inspired modeling chemistry. The pincer ligand is an excellent one to model biological activity since the N-

donor pyridine, like N-histidine, is sp^2-hybridized and thioimidazolyl sulfur donors have been reported by Parkin and Vahrenkamp to model thiol derived ligands in bio-inspired zinc chemistry [18, 19].

Toward the goal of synthesizing and understanding bio-inspired model complexes for the liver alcohol dehydrogenase active site, we report herein the syntheses, spectroscopic and electrochemical characterization, density functional theory (DFT) calculations and activity screening of tridentate SNS zinc pincer complexes.

2. Experimental:

2.1 General Procedures:

All reagents used are commercially available and were used as received. Isopropyl imidazole, neopentyl imidazole, 2,6-bis(3-butylimidazol-1-yl)pyridine bromide, 2,6-bis(3-isopropylimidazol-1-yl)pyridine bromide, and 2,6-bis(3-isopropylimidazol-2-thione-1-yl)pyridine were prepared as reported previously [20-24] as were BNA^+ and BNAH [25]. NMR spectra were recorded at 25 ^oC on a Bruker Avance 300 MHz NMR spectrometer. Spectra were referred to the solvent residual peak. Electrospray mass spectrometry was performed on a Micromass ZQ instrument using nitrogen as the drying and nebulizing gas. Cyclic voltammetry experiments were performed using a Cypress Electroanalytical System with a silver wire reference electrode, a glassy carbon working electrode, and a platinum counter electrode. The supporting electrolyte for the cyclic voltammetry experiments was tetra-N-butylammonium tetrafluoroborate. The ferrocenium/ferrocene couple was used as an internal reference; reduction potential values were corrected by assigning the

ferrocenium/ferrocene couple to 0.40 V versus SCE. When an inert atmosphere was needed, a M-Braun inert atmosphere glove box and standard Schlenk techniques were used with thoroughly degassed solvents. IR spectra were collected using a Thermo Nicolet AVATAR 380-FT-IR with a SMART SPECULATR reflectance adaptor. C, H, N elemental analyses were performed by Atlantic Microlab Inc. (Norcross, GA). Melting points are uncorrected.

2.2 Crystallographic Analyses:

Crystals of **1**, **2**, and **3** were mounted on a glass fiber or loop and placed in a -80 ^{o}C nitrogen stream on a Bruker diffractometer equipped with a Smart CCD at Boston College (Chestnut Hill, MA). Crystallographic data were collected using graphite monochromated 0.71073 Å Mo-Kα radiation and integrated and corrected for absorption using the Bruker SAINTPLUS software package. The structures were solved using direct methods and refined using least-square methods on F-squared. All other pertinent crystallographic details such as h, k, l ranges, 2θ ranges, and R-factors can be found in table 1.

Table 1. Crystal and Structure Refinement Data for **1-3**

	R = *i*Pr (**1**)	R = Np (**2**)	R = *n*Bu (**3**)
Formula	$C_{17}H_{22}Cl_4N_5OS_2Zn_2$	$C_{21}H_{30}Cl_4N_5OS_2Zn_2$	$C_{19}H_{25}Cl_4N_5S_2Zn_2$
FW (g/mol)	649.06	705.16	660.10
Temperature (K)	193(2)	193(2)	193(2)
Wavelength (Å)	0.71073	0.71073	0.71073
Crystal System	Monoclinic	Triclinic	Monoclinic
Space Group	P2(1)/c	P-1	P2(1)/c
a (Å)	7.475(2)	7.6011(19)	16.5135(6)
b (Å)	27.456(8)	13.297(3)	12.5308(5)
c (Å)	12.705(3)	14.952(4)	12.7522(5)
α (^{o})	90	96.534(5)	90
β (^{o})	98.163(6)	97.139(5)	94.713(2)
γ (^{o})	90	102.721(5)	90
Volume (Å)^3	2580.9(12)	1447.1(6)	2629.86(18)
Z	4	2	4
r (calc) (g/cm^3)	1.670	1.618	1.667
Abs (mm^{-1})	2.454	2.196	2.407
F(000)	1308	718	1336
Crystal Size (mm^3)	0.10 x 0.02 x 0.02	0.10 x 0.05 x 0.02	0.12 x 0.02 x 0.02
Theta Range (^{o})	1.48 to 28.36	1.39 to 28.39	1.24 to 27.57
Refl/Uniq	31809/6362	18174/6979	23665/6059
R(int)	0.1605	0.0692	0.0398
Abs Correction	None	None	None
Max./Min.	0.9526/0.7914	0.9574/0.8103	0.9534/0.7610
Ref Method	Full Matrix least squares on F^2	Full Matrix least squares on F^2	Full Matrix least squares on F^2
Data / restr / par	6362 / 0 / 286	6979 / 0 / 323	6059/ 0/ 291
GOF on F^2	1.122	1.092	0.790
R1 indices (I>2s)	0.0884	0.0636	0.0333
wR2	0.1577	0.1376	0.0806
Peak/hole (e/Å^{-3})	0.821 and -0.959	0.835 and -0.742	0.577 and -0.382

2.3 Reactivity:

In a typical reaction, 0.1 mmol of 4-nitrobenzaldehyde, 0.2 mmol of BNAH, and 0.1 mmol of the zinc complex or 0.2 mmol $ZnCl_2$ were dissolved in 3 mL of $CDCl_3$. The reaction was heated at reflux. Aliquots of the reaction were taken at certain times and analyzed using ^{1}H NMR spectroscopy. All data are averages of at least two runs.

2.4 Gaussian Calculations:

Gaussian 03 was used to perform single-point calculations and DFT geometry optimizations using the B3LYP hybrid functional with 6-31G* basis sets as provided with the software [26]. Calculations were performed on the pincer ligand precursor alone as well as on the bound Zn(II) system (R = Me in all cases). Symmetry was imposed on the metal-ligated complex such that one pseudo-tetrahedral (C_s) and two pseudo-square planar (C_2 and C_{2v}) structures were examined. In accordance with the molecular point groups, the SNS ligand set was required to be flat under C_{2v} symmetry, but could become nonplanar under C_2 or C_s symmetries. Frequency analysis was performed on the optimized structures to determine whether or not they represented true minima. We found no imaginary frequencies for the pseudo-tetrahedral structures, but we did find several for the pseudo-square planar systems as indicated in the discussion that follows.

Gas-phase geometry optimizations and single-point calculations using a solvent model were also performed on the unbound pincer ligand precursor in an effort to model the oxidation potentials that have been determined experimentally. After the structures of the ligand precursor were optimized in neutral and singly cationic and anionic states under each of the point groups described above, single-point SCRF calculations using DMSO via the CPCM solvent model were performed. The "radii=uff" and "nosymmcav" directives were employed. Oxidation and reduction potentials were then determined by finding the difference in the total free energies in solution for the neutral and cationic or anionic species. These ΔG values were then referenced to the absolute SCE potential in DMSO by subtracting 3.83V (the established correction [27] to SHE in DMSO) and 0.241 V (the difference between SHE and SCE).

2.5 Syntheses:

2.5.1 Preparation of 2,6-bis(3-neopentylimidazol-1-yl)pyridine bromide ($C_{21}H_{31}N_5Br_2$) [**2a**]:

In a round-bottom flask, 3.57 g (25.8 mmol) of neopentyl imidazole were added along with 3.20 g (13.5 mmol) of 2,6-dibromopyridine. The solution was brown and oily. The reaction mixture was heated neat at 160°C for 18 hours. After the reaction mixture was removed from the heat, the dark brown solid that remained in the round-bottom flask was dissolved in methanol (15 mL) the product was precipitated out of solution with 125 mL of diethyl ether. The tan crystals were collected by filtration through a Buchner funnel and were allowed to air dry. The yield was 3.07 g (44.3%). Melting point: 317-320 ^{o}C (dec). Anal calc. for $C_{21}H_{31}N_5Br_2 \cdot H_2O$ (531.33): C, 47.47; H, 6.26; N, 13.18. Found: C, 47.38; H, 6.23; N, 13.08.

^{1}H NMR (DMSO-d_6, 300 MHz) δ 10.85 ppm (s, 2H, imidazole CH), 8.93 ppm (s, 2H, imidazole CH), 8.62 ppm (m, 1H, pyridine CH), 8.34 ppm (d (^{3}J = 8.1 Hz), 2H, pyridine CH), 8.10 ppm (s, 2H, imidazole CH), 4.25 ppm (s, 2H, CH_2), 1.02 ppm (s, 18H, CH_3). ^{13}C {^{1}H} NMR (DMSO-d_6, 75MHz) δ 145.28 ppm (pyridine CH), 144.64 ppm (pyridine C), 136.23 ppm (imidazole CH), 125.14 ppm (imidazole CH), 119.11 ppm (imidazole CH), 114.29 ppm (pyridine CH), 59.99 ppm (CH_2), 32.08 ($C(CH_3)_3$), 26.69 ppm (CH_3).

2.5.2 Preparation of 2,6-bis(3-neopentylimidazol-2-thione-1-yl)pyridine, ($C_{21}H_{29}N_5S_2$) [**2b**]:

A 100mL round-bottom flask was charged with 0.52g (1.0 mmol) 2,6-bis(3-neopentylimidazol-1-yl)pyridine bromide, 0.20 g (2.4 mmol) sodium acetate and 40 mL

of acetonitrile . The solution was stirred at reflux for 30 minutes after which not all of the sodium acetate had dissolved. Then 0.66 g (21 mmol) sulfur was added to the round-bottom flask with an additional 10mL of acetonitrile. The solution was stirred at reflux for three days. The product was vacuum filtered to remove the remaining solids. The solvent was removed under reduced pressure. The yield (0.48 g) was quantitative. Electrospray MS (MeOH, 20V, positive ion mode (m/z): Expected: 415.2 (100 %) $[C_{21}H_{29}N_5S_2]^+$, Found: 416.5 (100%) $[C_{21}H_{29}N_5S_2+1]^+$. Anal calc. for $C_{21}H_{29}N_5S_2 \cdot H_2O$ (415.62): C, 58.17; H, 7.21; N, 16.15. Found: C, 57.58; H, 6.72; N, 15.80. ^{1}H NMR (DMSO-d_6, 300 MHz) δ 8.66 ppm (d (^{3}J = 8.1 Hz), 2H, pyridine CH), 8.19 ppm (t (^{3}J = 8.1 Hz), 1H, pyridine CH), 7.83 ppm (d (^{3}J = 2.4 Hz), 2H, imidazole CH), 7.33 ppm (d (^{3}J =2.7 Hz), 2H, imidazole CH), 4.00 ppm (s, 4H, CH_2), 1.00 ppm (s, 18H, CH_3), ^{13}C {^{1}H} NMR (DMSO-d_6, 75MHz) δ 163.07 ppm (C=S), 148.43 ppm (pyridine C), 139.77 ppm (pyridine CH), 119.99 ppm (imidazole CH), 117.35 ppm (pyridine CH), 116.19 ppm (imidazole CH), 56.58 ppm (CH_2), 33.75 ($C(CH_3)_3$), 27.86 ppm (CH_3). Selected IR bands (reflectance): ν_{max}/cm^{-1} 1125 (C=S).

2.5.3 Preparation of 2,6-bis[3-(*n*-butyl)imidazol-2-thione-1-yl]pyridine, ($C_{19}H_{25}N_5S_2$): [**3b**]

A round-bottom flask was charged with 0.48 g (1.0 mmol) of 2,6-bis[3-(*n*-butyl)imidazol-1-yl]pyridine bromide, 0.24 g (3.0 mmol) of sodium acetate and 40 mL of MeCN. The mixture was heated at reflux. After 30 minutes, 0.68 g (21 mmol) of sulfur was added. The reaction was heated at reflux for seven days. The product was vacuum filtered to remove the remaining solids. The solvent was removed under reduced

pressure. The yield was 0.38 g (70. %). Electrospray MS (MeOH, 20V, positive ion mode (m/z): Expected: 387.2 (100 %) $[C_{19}H_{25}N_5S_2]^+$, Found: 388.6 (100%) $[C_{19}H_{25}N_5S_2 +1]^+$. Anal calc. for $C_{19}H_{25}N_5S_2 \cdot 1.5H_2O$ (387.57): C, 55.04; H, 6.81; N, 16.89. Found: C, 55.22; H, 6.26; N, 16.73.

^{1}H NMR (DMSO-d_6, 300 MHz) δ 8.68 ppm (d (^{3}J = 7.8 Hz), 2H, pyridine CH), 8.20 ppm (t (^{3}J = 8.1 Hz), 1H, pyridine CH), 7.82 ppm (d (^{3}J = 2.4 Hz), 2H, imidazole CH), 7.42 ppm (d (^{3}J =2.7 Hz), 2H, imidazole CH), 4.05 ppm (t (^{3}J = 7.6 Hz), 4H, CH_2), 1.73 ppm (m, 4H, CH_2), 1.33 ppm (m, 4H, CH_2), 0.93 ppm (t (^{3}J = 7.5 Hz), 6H, CH_3). ^{13}C {^{1}H} NMR (DMSO-d_6, 75MHz) δ 161.26 ppm (C=S), 148.27 ppm (pyridine C), 139.90 ppm (pyridine CH), 118.86 ppm (imidazole CH), 116.99 ppm (pyridine CH), 116.47 ppm (imidazole CH), 46.47 ppm (CH_2), 29.96 (CH_2), 19.19 (CH_2), 13.54 ppm (CH_3). Selected IR bands (reflectance): ν_{max}/cm^{-1} 1126 (C=S).

2.5.4 Preparation of chloro(η^3-S,S,N)-[2,6-bis(3-isopropylimidazol-2-thione-1-yl)]pyridinezinc(II) aquatrichlorozincate, *($[C_{17}H_{21}N_5S_2ZnCl][ZnCl_3(OH_2)]$)* : **[1]**

In a 100mL round-bottom flask, 0.062 g (0.17mmol) 2,6-bis(3-isopropylimidazol-2-thione-1-yl)pyridine was combined with 0.057g (0.42mmol) $ZnCl_2$ and dissolved in 10mL CH_2Cl_2. The solution was stirred at reflux for 18h and the off-white solid was collected by vacuum filtration. The yield for the reaction was 0.070g (63%). Single crystals for X-ray diffraction were grown by a slow vapor diffusion of diethyl ether into a dichloromethane solution containing the zinc complex. Electrospray MS (MeOH, 0 V, positive ion mode (m/z)): Expected: 460.0 (99 %) $[C_{17}H_{21}N_5S_2ZnCl]^+$, Found: 459.9

(100%) [$C_{17}H_{21}N_5S_2ZnCl$]$^+$. Anal calc. for $C_{17}H_{23}Cl_4N_5OS_2Zn_2$ ·MeOH·2H_2O (718.17): C, 30.10; H, 4.35; N, 9.75. Found: C, 30.00; H, 3.91; N, 9.48.

^{1}H NMR (DMSO-d_6, 300 MHz) δ 8.64 ppm (d (^{3}J = 8.1 Hz), 2H, pyridine CH), 8.19 ppm (t (^{3}J = 8.1 Hz), 1H, pyridine CH), 7.84 ppm (d (^{3}J = 2.7 Hz), 2H, imidazole CH), 7.52 ppm (d (^{3}J =2.7 Hz), 2H, imidazole CH), 5.02 ppm (m, 2H, isopropyl CH), 1.35 ppm (d (^{3}J = 6.6 Hz), 12H, isopropyl CH_3). ^{13}C {^{1}H} NMR (DMSO-d_6, 75MHz) δ 160.53 ppm (C=S), 148.16 ppm (pyridine C), 140.00 ppm (pyridine CH), 117.48 ppm (imidazole CH), 117.17 ppm (pyridine CH), 115.25 ppm (imidazole CH), 48.12 ppm (isopropyl CH), 21.00 ppm (isopropyl CH_3).

^{1}H NMR (MeOD-d_3, 300 MHz) δ 8.72 ppm (d (^{3}J = 8.1 Hz), 2H), 8.15 ppm (m, 1H), 7.70 ppm (d (^{3}J = 2.7 Hz), 2H), 7.33 ppm (d (^{3}J =2.7 Hz), 2H), 5.21 ppm (m, 2H, isopropyl CH), 1.19 ppm (d (^{3}J = 7.2 Hz), 12H, isopropyl CH_3).

2.5.5 Preparation of chloro(η^3-S,S,N)-[2,6-bis(3-neopentylimidazol-2-thione-1-yl)]pyridinezinc(II) aquatrichlorozincate *[$C_{21}H_{27}N_5S_2ZnCl$][$ZnCl_3(OH_2)$]*: **[2]**

In a round-bottom flask, 0.14 g (0.35 mmol) of 2,6-bis(3-neopentylimidazol-2-thione-1-yl)pyridine was added to 0.10 g (0.73 mmol) of $ZnCl_2$. The reactants were dissolved in 8 mL of dichloromethane. The yellow solution was heated at reflux for 18 hours. An off-white precipitate was present at the end of the reaction. The solvent was removed under reduced pressure. Single crystals for X-ray diffraction were grown by a slow vapor diffusion of pentane into a dichloromethane solution containing the zinc complex. The yield for the synthesis was 0.24 g (quantitative). Electrospray MS (MeOH, 0 V, positive ion mode (m/z): Expected: 514.0 (100 %) [$C_{21}H_{27}N_5S_2ZnCl$]$^+$, Found: 514.3 (100%)

[$C_{21}H_{27}N_5S_2ZnCl$]$^+$. Anal calc. for $C_{21}H_{31}Cl_4N_5OS_2Zn_2 \cdot CH_3CN \cdot Et_2O$ (706.21): C, 39.48; H, 5.40; N, 10.23. Found: C, 39.21; H, 5.21; N, 10.75.

^{1}H NMR (DMSO-d_6, 300 MHz) δ 8.66 ppm (d (^{3}J = 8.1 Hz), 2H, pyridine CH), 8.19 ppm (t (^{3}J = 8.1 Hz), 1H, pyridine CH), 7.83 ppm (d (^{3}J = 2.4 Hz), 2H, imidazole CH), 7.33 ppm (d (^{3}J =2.1 Hz), 2H, pyridine CH), 4.00 ppm (s, 4H, CH_2), 1.00 ppm (s, 18H, CH_3). ^{13}C {^{1}H} NMR (DMSO-d_6, 75MHz) δ 163.08 ppm (C=S), 148.46 ppm (pyridine C), 139.32 ppm (pyridine CH), 120.04 ppm (imidazole CH), 117.42 ppm (pyridine CH), 116.24 ppm (imidazole CH), 56.61 ppm (CH_2), 33.78 ($C(CH_3)_3$), 27.89 ppm (CH_3). ^{1}H NMR (MeOD-d_3, 300 MHz) δ 8.64 ppm (d (^{3}J = 8.1 Hz), 2H, pyridine CH), 8.14 ppm (m, 1H, pyridine CH), 7.69 ppm (d (^{3}J = 2.4 Hz), 2H, imidazole CH), 7.23 ppm (d (^{3}J =2.1 Hz), 2H, imidazole CH), 4.08 ppm (s, 4H, CH_2), 1.05 ppm (s, 18H, CH_3).

2.5.6 Preparation of chloro(η^3-S,S,N)-{2,6-bis[3-(*n*-butyl)imidazol-2-thione-1-yl]}pyridinezinc(II) aquatrichlorozincate, *([$C_{19}H_{25}N_5S_2ZnCl$][$ZnCl_3$])* : [3]

In a round-bottom flask, 0.15g (0.38 mmol) of 2,6-bis[3-(*n*-butyl)imidazol-2-thione-1-yl]pyridine were combined with $ZnCl_2$, 0.099 g (0.73mmol), and dissolved in 10mL of CH_2Cl_2. The solution was refluxed for 18 h. An off-white precipitate was present at the end of the reaction. The solvent was removed under reduced pressure. Single crystals for X-ray diffraction were grown by a slow vapor diffusion of pentane into a dichloromethane solution containing the zinc complex. The yield was 0.25 g (quantitative). Electrospray MS (MeOH, 0 V, positive ion mode (m/z): Expected: 486.0 (100 %) [$C_{19}H_{25}N_5S_2ZnCl$]$^+$, Found: 486.4 (100%) [$C_{19}H_{25}N_5S_2ZnCl$]$^+$. Anal calc. for

$C_{19}H_{27}Cl_4N_5OS_2Zn_2 \cdot 0.5CH_3CN$ (678.15): C, 34.38; H, 4.11; N, 11.03. Found: C, 34.33; H, 4.17; N, 10.54.

^{1}H NMR (DMSO-d_6, 300 MHz) δ 8.68 ppm (d (^{3}J = 8.1 Hz), 2H, pyridine CH), 8.20 ppm (t (^{3}J = 8.1 Hz), 1H, pyridine CH), 7.82 ppm (d (^{3}J = 2.1 Hz), 2H, imidazole CH), 7.42 ppm (d (^{3}J =2.1 Hz), 2H, imidazole CH), 4.06 ppm (t (^{3}J = 7.2 Hz), 4H, CH_2), 1.73 ppm (m, 4H, CH_2), 1.34 ppm (m, 4H, CH_2), 0.93 ppm (t (^{3}J = 7.2 Hz), 6H, CH_3). ^{13}C {^{1}H} NMR (DMSO-d_6, 75MHz) δ 161.26 ppm (C=S), 148.27 ppm (pyridine C), 139.93 ppm (pyridine CH), 118.88 ppm (imidazole CH), 117.04 ppm (pyridine CH), 116.50 ppm (imidazole CH), 46.48 ppm (CH_2), 29.97 (CH_2), 19.19 (CH_2), 13.55 ppm (CH_3).

^{1}H NMR (MeOD-d_3, 300 MHz) δ 8.64 ppm (d (^{3}J = 8.1 Hz), 2H, pyridine CH), 8.17 ppm (m, 1H, pyridine CH), 7.70 ppm (d (^{3}J = 2.7 Hz), 2H, imidazole CH), 7.26 ppm (d (^{3}J =2.7 Hz), 2H, imidazole CH), 4.16 ppm (m, 4H, CH_2), 1.83 ppm (m, 4H, CH_2), 1.42 ppm (m, 4H, CH_2), 1.03 ppm (m, 6H, CH_3).

3. Results and Discussion:

3.1 Syntheses and Spectroscopy

The syntheses of the tridentate SNS ligand precursors and zinc pincer complexes **1-3** were accomplished following Scheme 1. The alkyl imidazoles were either prepared following known routes or were commercially available [20, 22]. Different R groups were employed because Crabtree has reported that modification of such substituents affects the solubility and catalytic activity of the metal complexes [23]. The alkyl imidazoles react neatly with 2,6-dibromopyridine to form the ligand precursor salts **1a, 2a,** or **3a** [28], which are soluble in DMSO, methanol, acetonitrile and water.

Compounds **1a, 2a,** and **3a,** react with a mild base, sodium acetate, and elemental sulfur in refluxing acetonitrile to form the bis-thione ligand precursors **1b, 2b,** and **3b**, respectively [24]. Instead of sodium acetate, a stronger base, potassium t-butoxide, could also be utilized [29]. As determined by NMR spectroscopy, **1b, 2b,** or **3b** can be purified by filtering a dichloromethane solution containing this compound through alumina. These compounds are soluble in DMSO, dichloromethane, chloroform, acetone, acetonitrile, and methanol.

The bis-thione ligand precursors subsequently react with $ZnCl_2$ in refluxing CH_2Cl_2 to afford compounds **1-3**. The driving force for the metallation is the formation of zinc complexes **1-3**, which are sparingly soluble in CH_2Cl_2. Off-white crystals that were suitable for x-ray diffraction were grown by allowing diethyl ether (**1**) or pentane (**2, 3**) to slowly diffuse into a dichloromethane solution containing **1, 2** or **3**. All of the reactions could be carried out in air, and the reactions proceeded in 63% to quantitative yield. The zinc complexes **1-3** are soluble in dimethyl sulfoxide, acetonitrile, methanol, and water and are sparingly soluble in dichloromethane and chloroform.

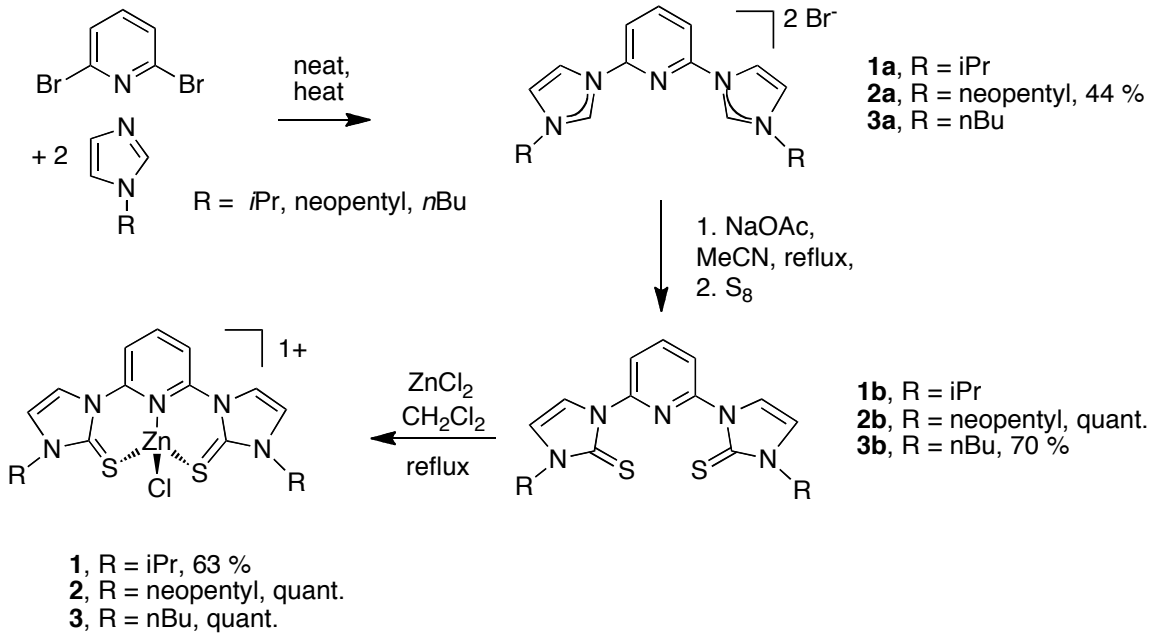

Scheme 1: Preparation of **1-3**

Ligand precursors **1a**, **1b**, **2a**, **2b**, **3a**, and **3b** were characterized using ^{1}H, ^{13}C, and HSQC NMR spectroscopy. For these ligand precursors and zinc complexes **1-3**, only one set of resonances was detected indicating that the two halves of each molecule are symmetry-related. The ^{13}C NMR spectra of **1b**, **2b**, and **3b**, show resonances at ~161 ppm that are consistent with C=S formation [17]. The bis-thione ligand precursors, **1b**, **2b**, and **3b**, lacked the acidic C-H proton at δ ~11 ppm in the ^{1}H NMR spectra, whereas this proton resonance was present for the precursors **1a, 2a,** and **3a**.

Complexes **1-3** were analyzed with ^{1}H, ^{13}C, and HSQC NMR spectroscopy in DMSO-d_6. The ^{1}H and ^{13}C NMR spectra of the zinc complexes **1-3** are largely the same with very little shift in the resonances when compared to the respective ligand precursors **1b**, **2b**, and **3b**. This was expected since no hydrogen or carbon atoms are displaced or added upon metallation with zinc(II) chloride. In addition, the ^{1}H NMR spectra of complexes **1-**

3 were acquired in a less polar and weakly coordinating solvent, MeOD-d_3, to verify that the SNS pincer ligands cannot be displaced from the coordination sphere of zinc. Electrospray mass spectrometry data, described below, also verifies this result. Zinc complexes **1**-**3** are sparingly soluble in MeOD-d_3. When compared to the ^{1}H NMR spectra of complexes **1-3** that were acquired in DMSO-d_6, there was a slight shift (δ ~0.05 to 0.10) ppm of all of the resonances in the proton NMR spectra that were acquired in MeOD-d_3. In the ^{1}H NMR spectra that were acquired in MeOD-d_3, when compared to the ^{1}H NMR spectra acquired in DMSO-d_6, some of the resonances shifted upfield while others shifted downfield.

ESI-MS spectra for compounds **1**-**3** were collected with cone voltages of 0 V and 70 V. The predominant feature in the spectra of these systems at the higher cone voltage is that of the fully ligated zinc complex, indicating that the compound is stable and suggesting that it is unlikely that the ligand is displaced when dissolved in a polar solvent. In negative ion mode, the expected m/z values were seen for $[ZnCl_3]^-$. The isotopic patterns in the mass spectrometry data fit the assigned structures.

3.2 X-ray Crystallography

The solid-state molecular structures of **1**, **2**, and **3** are shown in Figure 1. Complexes **1-3** feature SNS donor atoms and pseudotetrahedral geometry about the zinc center, as is seen for liver alcohol dehydrogenase. The bond lengths and bond angles for **1-3** are listed and are compared to the active site in horse LADH-CNAD in Table 2. CNAD is an isoteric C-glycosidic analogue of NADH containing a neutral pyridine ring, which is a potential inhibitor of LADH. During catalysis, it is proposed that cofactor and substrate

are near the zinc(II) active site [32]. In the LADH-CNAD structure, the CNAD mimics the cofactor binding to LADH. Therefore, we selected this crystal structure because this structure contained a co-factor mimic and an ethanol molecule in the active site. The bond lengths and bond angles for **1-3** compare reasonably well to LADH-CNAD. The carbon-sulfur bond lengths of ~1.7 Å are between what is normally associated with a C-S single bond, 1.83 Å, and a C=S double bond, 1.61 Å [30]. For **1** and **2**, the counter-anion is $[ZnCl_3(H_2O)]^-$ and for **3**, the counter ion is $[ZnCl_3]^-$. The counter-ion is seen even when either one or two molar equivalents of $ZnCl_2$ are used in the preparation of **1-3**.

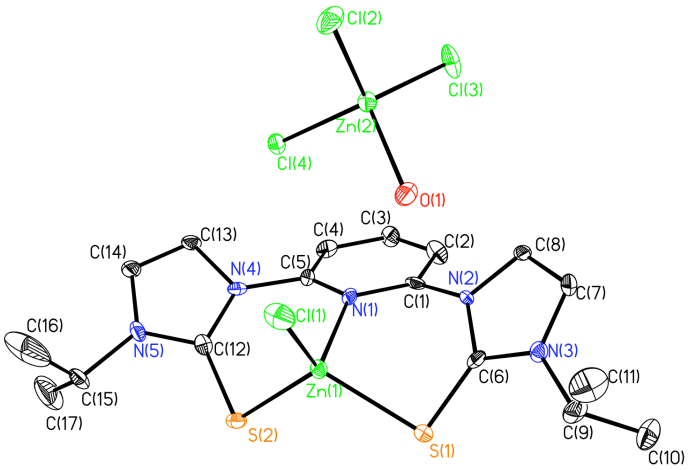

(1)

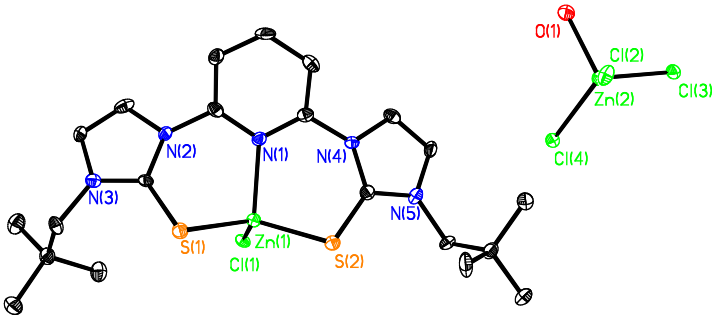

(2)

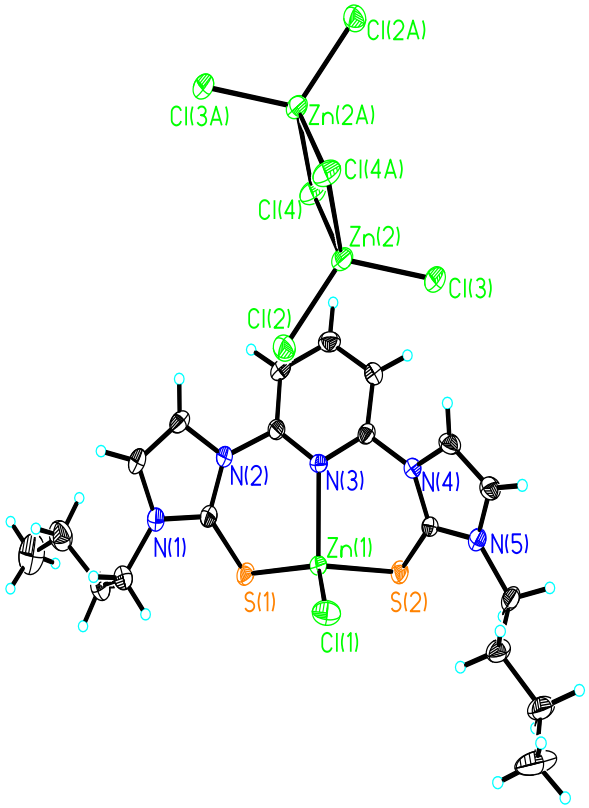

(3)

Figure 1. Solid-state structures of complexes **1-3**.

Table 2. Selected bond lengths and angles (esd) for 1-3 and comparison to LADH-CNAD [31]

	R = *i*Pr (**1**)	R = neopentyl (**2**)	R = *n*Bu (**3**)	LADH-CNAD[a]
Zn(1) – N(1) (Å)	2.091(6)	2.101(5)	2.145(2)	2.0
Zn(1) – Cl(1) (Å)	2.210(2)	2.2301(15)	2.1930(9)	2.2[a]
Zn(1) – S(1) (Å)	2.303(2)	2.2937(16)	2.2822(9)	2.3
Zn(1) – S(2) (Å)	2.307(2)	2.3146(16)	2.3431(9)	2.3
S(1) – C(6) (Å)	1.710(8)	1.706(5)	1.710(3)	
N(1) – Zn(1) – Cl(1)	111.96(17)	111.80(13)	113.92(7)	136
N(1) – Zn(1) – S(2)	96.66(17)	97.83(13)	94.07(7)	106
Cl(1) – Zn(1) – S(2)	117.01(8)	118.76(13)	108.92(4)	97[a]
N(1) – Zn(1) – S(1)	95.53(17)	94.98(13)	96.01(7)	97
Cl(1) – Zn(1) – S(1)	120.44(9)	117.41(6)	123.85(4)	98[a]
S(2) – Zn(1) – S(1)	110.36(8)	111.46(6)	115.26(3)	125

[a] Instead of Cl atom in LADH-CNAD, this entry refers to $N5_N$ atom of CNAD pyridine ring.

3.3 Cyclic Voltammetry of Ligand Precursors and Comparison of Cyclic Voltammetry Results to Gaussian Calculations.

The bis-thione ligand precursor, **2b**, was studied by cyclic voltammetry, as part of its characterization. This compound shows a reversible oxidation wave at 1289 mV and a reduction wave at -2367 mV by cyclic voltammetry in DMSO (Figure 2). The oxidation and reduction occurred at the same potential when two consecutive cycles were collected.

Thus, the ligand precursor itself is stable with respect to repeated oxidations and reductions. We performed Gaussian calculations to further understand our cyclic voltammetry results.

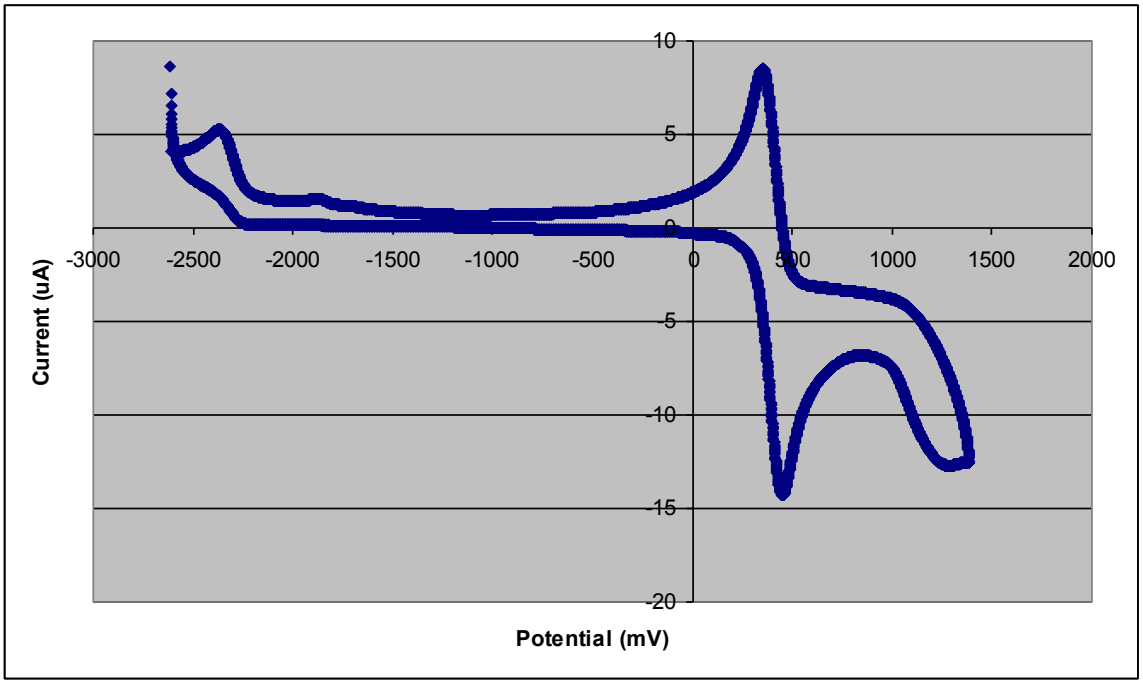

Figure 2. Cyclic Voltammogram of **2b** in DMSO (2mM) with 0.2 M TBAF. The scan rate was 100 mV/s with ferrocene ($E_{1/2}$ = 400 mV) used as an internal standard.

Our Gaussian calculations agree quite well with the experimentally observed oxidation potential for the pincer ligand precursor. Under the various point groups considered, the computed ΔG values are 1297 mV (C_s), 1304 mV (C_2), and 1420 mV (C_{2v}). While all three of these potentials are close to that found experimentally (1289 mV), the ΔG value found when the ligand is modeled under C_s symmetry is the closest. As can be seen from the contour plot of the HOMO shown in Figure 3, the electron is removed from a π-type orbital that is largely based on the thioimidazolyl portions of the molecule. Upon oxidation, the main structural change observed in the optimized structures is an increase in the dihedral angle between the thioimidazolyl and pyridinyl

sections of the molecule. Under C_s symmetry, the dihedral angle is determined to be 21.3º for the neutral system and 38.5º for the cation, which indicates that the sulfur atoms are closer to each other in the oxidized compound than in the neutral system. Given that the sulfurs of the thioimidazole rings are closest to each other under C_s symmetry than under the C_2 or C_{2v} point groups and that similar systems are known to form disulfides upon oxidation [33], the excellent agreement between the experimental oxidation potential (1289 mV) and the value calculated by Gaussian (1297 mV) indicates an acceptable level of modeling for this system.

As for the one-electron reduction of the pincer ligand, the computed ΔG values (-5734 mV (C_s), -5720 mV (C_2), and -5748 mV (C_{2v})) do not match the potential observed experimentally (-2367 mV), suggesting that the reduction wave does not correspond with a simple one-electron reduction of the ligand precursor. The contour plot of the LUMO, shown in Figure 3, indicates that the electron is added into a π-type orbital that is distributed across all portions of the molecule. Upon reduction, the ligand is flat with a calculated thioimidazolyl-pyridinyl dihedral angle of 0.0º, which can be understood through consideration of the N-C π bonding nature between the thioimidazolyl and pyridinyl fragments of the molecule.

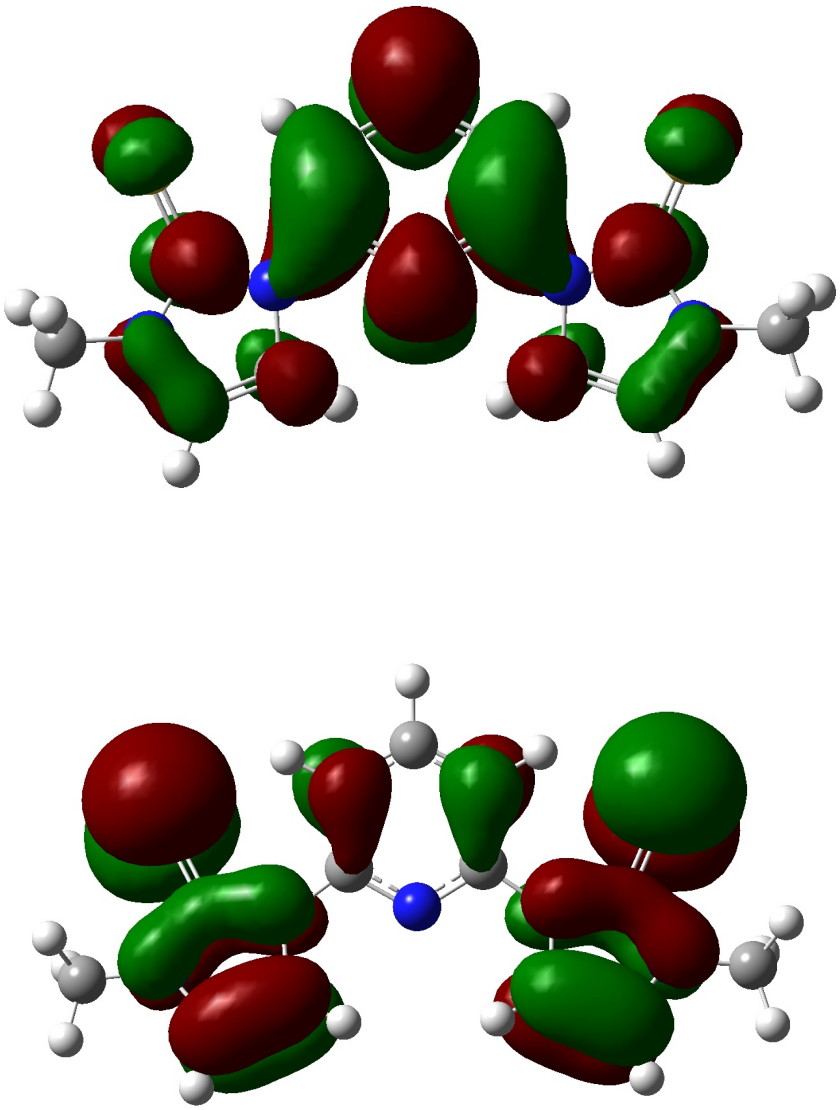

Figure 3. Orbital contour plots for the LUMO (top) and HOMO (bottom) of the methyl-substituted analogue of **2b**.

3.4 Density Functional Theory Calculations to Understand Geometry About the Zinc Center

Because tridentate pincer ligand precursors are known to coordinate to metals in either a meridional or facial fashion, we were interested in understanding the energy

difference between a pseudo-tetrahedral complex (facial coordination of pincer ligand) and a pseudo-square planar complex (meridional coordination of pincer ligand) of this zinc pincer system. Pincer ligands have been reported to coordinate in a meridional fashion to d^8 Pd(II) and Pt(II) centers to yield systems that possess a pseudo-square planar environment at the metal center [17]. Given the ability of the ligand precursor systems **1b**, **2b**, and **3b** to establish π-conjugation across multiple rings when flat, we were interested in understanding whether such electronic influences would enforce a square planar environment upon the metal center or if the preference of d^{10} Zn(II) to attain a tetrahedral coordination sphere would predominate.

Our calculations show that a pseudo-tetrahedral geometry is preferred for a d^{10} zinc system with a ligand precursor set that is analogous to that found in complexes **1-3** (Figure 1 and Table 1). The system with the Zn center in a pseudo-square planar environment and C_2 molecular geometry overall is calculated to be 18.3 kcal/mol less stable than the pseudo-tetrahedral structure as depicted in Figure 4. The pseudo-square planar system with C_{2v} symmetry is 43.8 kcal/mol less stable than the pseudo-tetrahedral structure. Analysis of the C_2 system finds that it has one vibration with an imaginary frequency (28.03i), the C_{2v} system possesses four (44.16i, 62.88i, 123.07i, and 138.96i cm^{-1}), and the C_s system has none in agreement with the observation of pseudo-tetrahedral systems for compounds **1-3**. Visualization with GaussView of several of the imaginary frequencies for the C_{2v} system shows that they represent torsion of the ligand set away from being planar and toward the geometry adopted in the pseudo-tetrahedral structure.

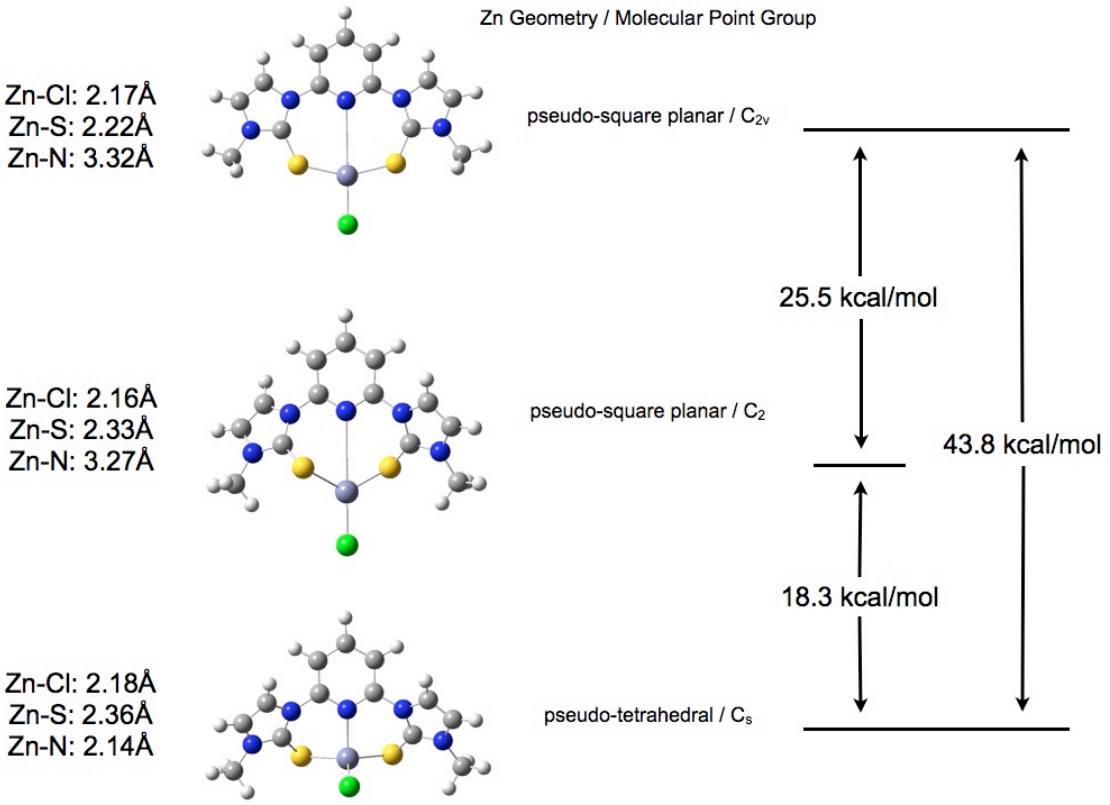

Figure 4. Optimized pseudo-tetrahedral and pseudo-square planar structures from DFT calculations. Select optimized bond distances are provided.

Various bond lengths and angles found in the three optimized structures are worth note. The Zn-S, Zn-Cl, and Zn-N bond lengths of the pseudo-tetrahedral structure are in good agreement with those given for **1-3** in Table 1. Constraining the pincer precursor ligand to be planar to enforce a pseudo-square planar environment around the Zn center under C_{2v} symmetry requires the Zn-N bond length to elongate to 3.32Å, which is nearly 1.2 Å longer than was calculated for the pseudo-tetrahedral structure. Furthermore, the bond angles at the Zn center (N-Zn-S 76.9º) show that the donor atoms are reasonably

well aligned with the filled Zn d_{x2-y2} orbital, thereby providing instability to this structure. The pseudo-square planar system with C_2 symmetry has a Zn-N bond of a similar length (3.27 Å), but given that the ligand can flex more freely than it can under C_{2v} symmetry, the optimized N-Zn-S bond angle of 65.1º allows relaxation of the σ-donor atoms away from the Zn d_{x2-y2} orbital and therefore a more stable structure than found for the C_{2v} system.

We next chose to calculate the energy differences between the pseudo-tetrahedral and pseudo-square planar systems with the ligand set split into three monodentate fragments. Doing so allows us to separate the influence of the d^{10} electronic population of the metal center from the coordination environment imposed by a unified tridentate SNS ligand precursor set. Shown in Figure 5 are the optimized pseudo-tetrahedral and pseudo-square planar structures in which the pyridine and imidazole fragments have been allowed to attain the most stable orientations possible within the constraints of the imposed molecular symmetries. In these structures, the pyridine rings are not connected to the imidazoles. No imaginary frequencies were found for the pseudo-tetrahedral C_s structure while five (18.32i, 21.91i, 24.28i, 28.34i, 45.73i cm^{-1}) were found for the C_{2v} pseudo-square planar system and four (7.77i, 9.81i, 19.52i, 52.57i cm^{-1}) were located for the C_2 pseudo-square planar system.

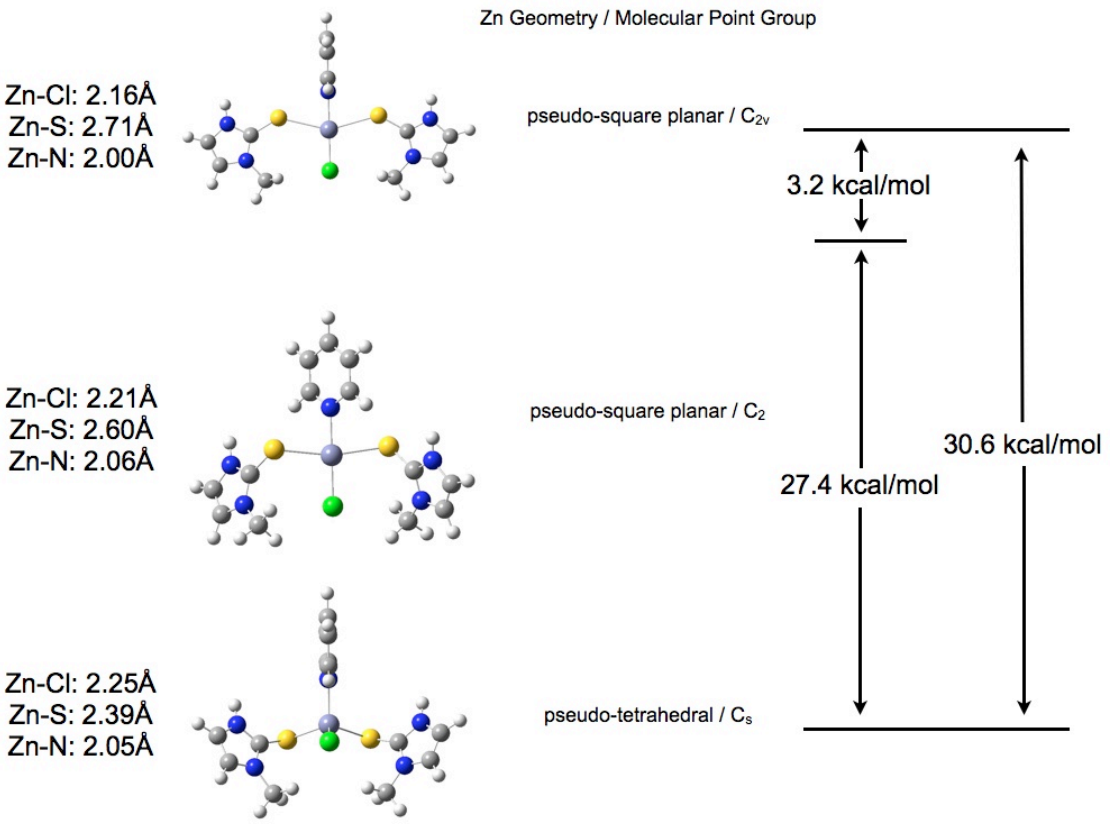

Figure 5. Optimized pseudo-tetrahedral and pseudo-square planar structures from DFT calculations with the pyridine ring and imidazole moities in optimal configurations. Select optimized bond distances are provided.

Comparison of the systems that contain monodentate ligands with those that have a tridentate ligand reveals interesting structural information. The calculated Zn-Cl, Zn-S, and Zn-N bond lengths for the pseudo-tetrahedral systems are quite similar under both ligand environments. However, the C_{2v} pseudo-square planar system has comparatively short Zn-N and long Zn-S bonds in the tridentate ligand environment while the structural constraints of the single tridentate ligand impose a long Zn-N bond and relatively short

Zn-S bonds on the molecule. The geometric requirements of a single, flat SNS ligand precursor therefore impose an additional 13.2 kcal/mol penalty (43.8 kcal/mol – 30.6 kcal/mol) upon the C_{2v} pseudo-square planar structure relative to the C_s pseudo-tetrahedral system.

On the whole, the relative stabilities of the pseudo-tetrahedral and pseudo-square planar systems are the same for this coordination environment about zinc whether the ligand set is a single tridentate SNS system or is broken into three separate units. The preference of a d^{10} Zn center to attain a tetrahedral local environment trumps any stabilization gained by removal of constraints within the ligand set.

3.5 Reactivity

Having established a synthetic protocol for these metalloenzyme models and gained an understanding of their structural characteristics, we turned our attention to probing their stoichometric activity. We chose 4-nitrobenzaldehyde, an electron-poor aldehyde, to screen the ability of **1-3** to reduce such a system in the presence of the hydrogen donor BNAH (eq. 1). BNAH was prepared following a known literature procedure and is the reagent of choice to model NADH [25]. ^{1}H NMR spectroscopy was used to follow the disappearance of the aldehyde proton (δ 10.2 ppm) and the shifting of the aromatic C-H protons in the alcohol product (δ 8.24 ppm). The aromatic proton resonance of the alcohol product did not overlap with the ^{1}H NMR resonances of either the starting materials or the products or the zinc complex. In all of the reactivity experiments, 0.1 mmol of aldehyde, 0.1 mmol zinc precursor or 0.2 mmol of $ZnCl_2$, and 0.2 mmol BNAH were used. When $ZnCl_2$ was added, the $ZnCl_2$ was the only zinc compound in the reaction mixture. In the control reactions, two equivalents of $ZnCl_2$ were used because in

complexes **1-3**, there are two zinc ions (one in the cation and one in the anion) ion per neutral compound. The products were detected by ^{1}H NMR by comparison with authentic material. In no case was there any indication of reduction of nitro substituents. Table 3 illustrates the reactivity data for **1-3** as well as for $ZnCl_2$ and the ligand precursor.

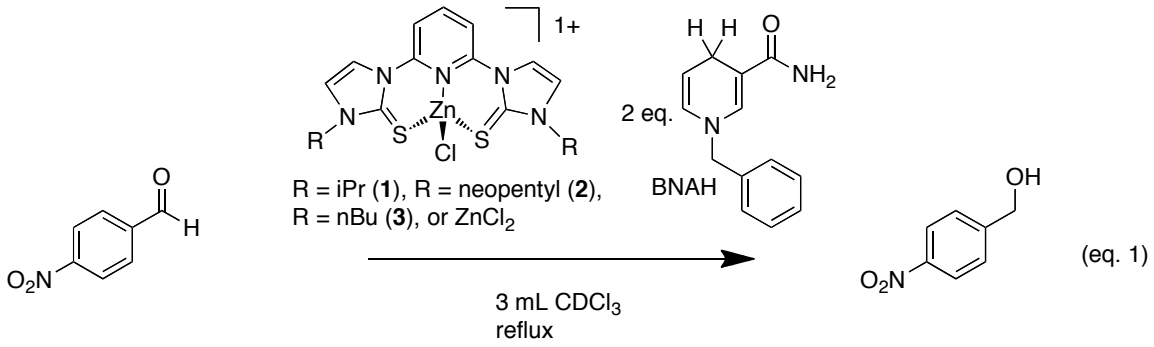

Table 3. Reactivity Data for **1-3**

Entry	Zn Complex	Time	Conversion (%)
1	None	20h	< 5
2	**2b** (bis thione ligand precursor)	20h	< 5
3	$ZnCl_2$ (2 eq.)	5h	15
4	$ZnCl_2$ [a] (2 eq.)	20h	13
5	$ZnCl_2$ (2 eq.)	20h	18
6	**1**	20h	42
7	**2**	20h	48
8	**3**	20h	33
9	$ZnCl_2$ (10 eq.)	20h	42

[a] Reaction was run under an N_2 environment. The reaction was performed in an inert atmosphere glove box.

As shown in Table 3, zinc complexes **1-3** enhance the rate of the reaction for the reduction of 4-nitrobenzaldehyde when compared to $ZnCl_2$ or ligand precursor. Based on a mechanism for LADH proposed by Berreau and co-workers, there is a hydrogen transfer between the co-factor and the substrate, which is coordinated to the zinc active site [32]. We also learned that $ZnCl_2$ reacts stoichiometrically with electron poor aldehydes such as 4-nitrobenzaldhyde to yield alcohol product to a small extent (ca. 18 % conversion). We suppose that Zn^{2+} acts as a Lewis acid catalyst in the reaction where $ZnCl_2$ is utilized. Perhaps, the Zn^{2+} in the counteranion contributes to the reactivity that is shown for **1-3** in Table 3. Experiments are underway to prepare tridentate zinc SNS pincer complexes with a counter-anion that does not contain a zinc ion. We also wondered if an excess of $ZnCl_2$ would enhance the rate of conversion of 4-nitrobenzaldehyde. We saw 42 % conversion of 4-nitrobenzaldehyde after 20 h when excess $ZnCl_2$ (10 eq) was used. Thus, an excess of $ZnCl_2$ and BNAH could be utilized to reduce 4-nitrobenzaldehyde.

Based on the data presented in Table 3, it appears that the choice of the R group is important as isopropyl and neopentyl groups gave a higher percent conversion than *n*-butyl. Larger R groups are needed to prepare zinc complexes that have increased solubility in organic solvents. The more sterically demanding *n*-butyl wingtip group, when compared to neopentyl or isopropyl, may shield the zinc metal center from interacting with BNAH and substrate. This is another example that illustrates that the

identity of the wingtip group is a very important variable to consider when screening metal complexes for activity [23].

We also tried to reduce another electron poor aldehyde, pyridine-2-carboxaldehyde, in the presence of a stoichiometric amount of **1** or $ZnCl_2$ (eq. 2).

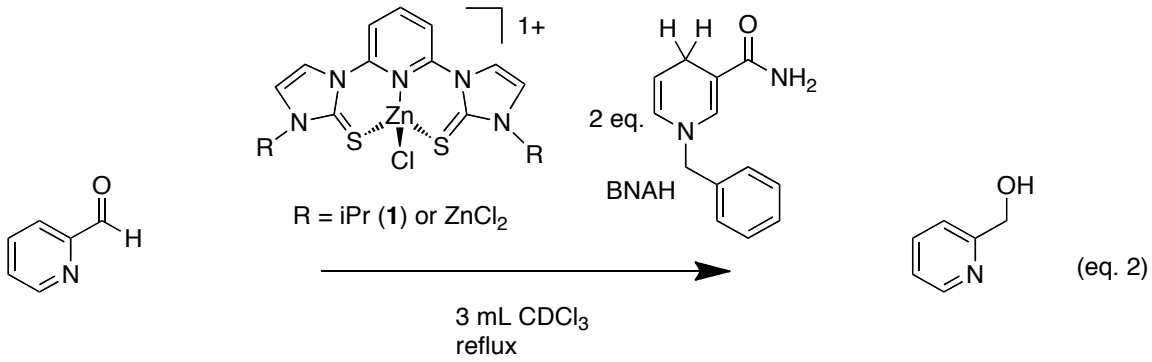

(eq. 2)

^{1}H NMR was used to follow the disappearance of the aldehyde proton (δ 10.2 ppm) and the shifting of the aromatic C-H protons in the alcohol product (δ 8.4 ppm). The aromatic proton resonance of the alcohol product did not overlap with the ^{1}H NMR resonances of either the starting materials or the products or the zinc complex. Table 4 illustrates the reactivity data for **1** as well as for $ZnCl_2$.

Table 4. Reactivity Data for **1** for the reduction of pyridine-2-carboxaldehyde.

Entry	Zn Complex	Time	Conversion (%)
1	None	20h	< 5
2	**1**	20h	35
3	$ZnCl_2$	20h	19

As shown in Table 4, zinc complex **1** enhances the rate of the reaction for the reduction of pyridine-2-carboxaldehyde when compared to $ZnCl_2$.

As seen in Tables 3 and 4, enhancement for the reduction of 4-nitrobenzaldehyde or pyridine-2-carboxaldehyde was observed for complexes **1**-**3**. Stoichiometric conversion to the alcohol product was not observed for either 4-nitrobenzaldehyde or pyridine-2-carboxaldehyde. Based on the mechanism proposed by Berreau and co-workers [32], the low activity of complexes **1**-**3** could be due to the slow hydrogen transfer between the co-factor and the substrate, which is coordinated to the zinc active site. More importantly, the alcohol product may inhibit the reaction. As the alcohol is formed, it may coordinate to the zinc metal center as the reaction progresses, and thereby hinder the reaction.

4. Conclusions

A series of Zn(II) compounds containing the SNS facial coordination of a tridentate pincer ligand was prepared and characterized. The tridentate SNS pincer ligand precursors and zinc complexes used in this work have provided new insights in the field of bioinorganic modeling chemistry. The zinc complexes serve as models for the zinc active site in liver alcohol dehydrogenase. The SNS zinc pincer complexes adopt pseudo-tetrahedral geometry and have a SNS coordination environment about the zinc center like LADH and react with BNAH to reduce electron poor aldehydes. The reactivity of **1**-**3** is not optimal when compared to LADH. It remains a challenge to synthesize a neutral zinc complex with a tridentate ligand with SNS donor atoms that yield reactivity that is comparable to LADH.

Gaussian calculations were performed to prove various structural and electronic properties of these compounds. The computed oxidation potentials matches well with what is observed experimentally while the calculated reduction potential indicates that

the experimental reduction wave does not correspond to a simple one-electron reduction of the ligand precursor without other reactivity occurring. DFT calculations were also performed to better understand why the geometry about the zinc center is pseudo-tetrahedral rather than pseudo-square planar, which is seen for most pincer complexes. Overall, the relative stabilities of the pseudo-tetrahedral and pseudo-square planar systems are the same for this coordination environment whether the ligand set is a single tridentate SNS system or is broken into three separate units. The preference of a d^{10} Zn center to attain a tetrahedral local environment trumps any stabilization gained by removal of constraints within the ligand set.

Supporting Information:

The ^{1}H, ^{13}C and HSQC NMR spectra of **2a**, **2b**, **3b**, and **1-3** and mass spectra of **1-3** are provided. IR spectra for **2b** and **3b** and crystallographic details of **1-3** are also given.

Acknowledgement:

This work was supported by generous funding from The Fairfield University Science Institute (JRM), Fairfield University Start-up Funding (JRM), a Fairfield University Research Grant (JRM), and a NTID Faculty Evaluation and Development Grant (MAL). JRM would like to thank Prof. Matthew A. Kubasik, Prof. L. Kraig Steffen, and Prof. Swapan Jain, for helpful suggestions.

References:

[1] R.H. Holm, P. Kennepohl, E.I. Solomon, Chem. Rev., 1996, 96, 2239-2314.

[2] J.A. Ibers, R.H. Holm, Science, 1980, 209, 223-235.

[3] (a) W.N. Lipscomb, N. Sträter, Chem. Rev. 1996, 96, 2375-2433. (b) E. Kimura, T. Koike, M. Shionoya, Structure and Bonding, 1997, 89, 1-28.

[4] K.K. Kannan, B. Nostrand, K. Fridborg, S. Lovgren, A. Ohlsson, M. Petef, Proc. Natl. Acad. Sci, USA, 1975, 72, 51.

[5] A. Meibner, W. Haehnel, H. Vahrenkamp, Chem. Eur. J, 1997, 3, 261-267.

[6] A. Dolega, Coord. Chem. Rev., 2010, 254, 916-937.

[7] A. Dolega, A. Pladzyk, K. Baranowska, J. Jezierska, Inorg. Chim. Acta, 2009, 362, 5085-5096.

[8] L. Cronin, P.H. Walton, Chem Commun, 2003, 1572-1573.

[9] L.M. Berreau, M.M. Makowska-Grzyska, A.M. Arif, Inorg Chem, 2001, 40, 2212-2213.

[10] R.M.Kellogg, R.P. Hof, J Chem Soc, Perkin Trans 1, 1996, 1651-1657.

[11] S.C. Shoner, K.J. Humphreys, D. Barnhart, J.A. Kovacs, Inorg. Chem, 1995, 34, 5933-5934.

[12] (a) B. Kaptein, G. Barf, R.M. Kellogg, F. Van Bolhuis, J. Org. Chem, 1990, 55, 1890-1891. (b) B. Kaptein, L.Wang-Griffen, G. Bart, R.M. Kellogg, J Chem. Soc Chem Commun, 1987, 1457-1459.

[13] D.T. Corwin, R. Fikar, S.A. Koch, Inorg. Chem, 1987, 26, 3079-3080.

[14] (a) C. Kimblin, T. Hascall, G. Parkin, Inorg. Chem., 1997, 36, 5680-568. (b) C. Kimblin, B.M. Bridgewater, D.G. Churchill, G. Parkin, Chem. Commun; 1999, 2301-2302.

[15] (a) R. Walz, H. Vahrenkamp, Inorg. Chim. Acta, 2001, 314, 58-62. (b) Y.H. Zhang, H. Vahrenkamp, Inorg. Chim. Acta, 2003, 351, 201-206.

[16] (a) M. Albrecht, G. van Koten, Angew. Chem. Int. Ed., 2001, 40, 3750-3781. (b) A.T. Normand, K.J. Cavell, Eur. J. Inorg. Chem., 2008, 2781-2800.

[17] D. Morales-Morales, C.M. Jensen, eds. The Chemistry of Pincer Compounds, Elsevier: New York, 2007.

[18] (a) C. Kimblin, T. Hascall, G. Parkin, Inorg. Chem., 1997, 36, 5680-568. (b) C. Kimblin, B.M. Bridgewater, D.G. Churchill, G. Parkin, Chem. Commu, 1999, 2301-2302. (c) C. Bergquist, G. Parkin, Inorg. Chem., 1999, 38, 422-423. (d) G. Parkin, Chem. Rev, 2004, 104, 699-767. (e) B.M. Bridgewater, T. Fillebeen, R.A. Friesner, G. Parkin, J. Chem. Soc., Dalton Trans, 2000, 4494-4496. (f) J.G. Melnick, A. Docrat, G.

Parkin, Chem. Commun, 2004, 2870-2871. (g) C. Kimblin, B.M. Bridgewater, D.G. Churchill, T. Hascall, G. Parkin, Inorg. Chem, 2000, 39, 4240-4243.

[19] (a) M. Tessmer, M. Shu, H. Vahrenkamp, Inorg. Chem., 2001, 40, 4022-4029. (b) J. Seebacher, M. Shu, H. Vahrenkamp, Chem. Commun; 2001, 1026-1027. (c) Y.H. Zhang, H. Vahrenkamp, Inorg. Chim. Acta, 2003, 351, 201-206. (d) M.M. Ibrahim, M. Shu, H. Vahrenkamp, Eur. J. Inorg. Chem, 2005, 1388-1397. (e) R. Walz, H. Vahrenkamp, H. Inorg. Chim. Acta, 2001, 314, 58-62. (f) M. Rombach, J. Seebacher, M. Ji, G. Zhang, G. He, M. Ibrahim, B. Benkmil, H. Vahrenkamp, Inorg. Chem, 2006, 45, 4571-4575. (g) M. Ibrahim, J. Seebacher, G. Steinfeld, H. Vahrenkamp, Inorg. Chem, 2005, 44, 8531-8538.

[20] Gridnev, A.A.; Mihaltseva, I.M. Synth. Commun., 1994, 24, 1547.

[21] J.A. Loch, M.A. Albrecht, E. Peris, J. Mata, J.W. Faller, R.H. Crabtree, Organomet., 2002, 21(4), 700-706.

[22] E. Kuwano, M. Kikuchi, M. Eto, Agricultural and Biological Chem, 1988, 52(6), 1619-1620.

[23] M. Albrecht, J.R. Miecznikowski, A. Samuel, J.W. Faller, R.H. Crabtree, Organomet, 2002, 21(17), 3596-3604.

[24] W.-G. Jia, Y.-B. Huang, G.-X. Jin, G-X. J. Organomet. Chem, 2009, 694 (25), 4008-4013.

[25] J. Lutz, F. Hollmann, T.V. Ho, A. Schnyder, R. Fish, A. Schmid, J. Organomet. Chem, 2004, 689, 4783-4790.

[26] M.J. Frisch, G.W. Trucks, H.B. Schlegel, G.E. Scuseria, M.A. Robb, J.R. Cheeseman, J. A. Montgomery Jr., T. Vreven, K.N. Kudin, J.C. Burant, J. M. Millam, S. S. Iyengar, J. Tomasi, V. Barone, B. Mennucci, M. Cossi, G. Scalmani, N. Rega, G.A. Petersson, H. Nakatsuji, M. Hada, M. Ehara, K. Toyota, R. Fukuda, J. Hasegawa, M. Ishida, T. Nakajima, Y. Honda, O. Kitao, H. Nakai, M. Klene, X. Li, J.E. Knox, H.P. Hratchian, J.B. Cross, V. Bakken, C. Adamo, J. Jaramillo, R. Gomperts, R.E. Stratmann, O. Yazyev, A.J. Austin, R. Cammi, C. Pomelli, J.W. Ochterski, P.Y. Ayala, K. Morokuma, G.A. Voth, P. Salvador, J.J. Dannenberg, V.G. Zakrzewski, S. Dapprich, A.D. Daniels, M.C. Strain, O. Farkas, D.K. Malick, A.D. Rabuck, K. Raghavachari, J.B. Foresman, J. V. Ortiz, Q. Cui, A.G. Baboul, S. Clifford, J. Cioslowski, B. B. Stefanov, G. Liu, A. Liashenko, P. Piskorz, I. Komaromi, R.L. Martin, D.J. Fox, T. Keith, M.A. Al-Laham, C.Y. Peng, A. Nanayakkara, M. Challacombe, P.M.W. Gill, B. Johnson, W. Chen, M.W. Wong, C. Gonzalez, J.A. Pople, Gaussian 03, Revision E.01; Gaussian, Inc.: Wallingford, CT, 2004.

[27] (a) W.R. Fawcett, Langmuir, 2008, 24, 9868. (b) L.E. Roy, E. Jakubikova, G. Guthrie, E.R. Batista, J. Phys. Chem. A, 2009, 113, 6745-6750.

[28] E. Peris, J.A. Loch, J. Mata, R.H. Crabtree, Chem Commun, 2001, 201-202.

[29] A. Caballero, E. Díez-Barra, F.A. Jalón, S. Merino, J. Tejeda, J. Organomet. Chem., 2001, 617-618, 395-398.

[30] B.V. Trzhtsinskaya, N.D. Abramova, J Sulfur Chemistry, 1991, 10(4), 389-421.

[31] H. Li, W.H. Hallows, J.S. Punzi, K.W. Pankiewicz, K.A. Watanabe, B.M. Goldstein, Biochemistry, 1994, 33, 11734-11744.

[32] M.M. Makowska-Grzyska, P.C. Jeppson, R.A. Allred, A.M. Arif, L.M. Berreau. Inorg. Chem, 2002, 41, 4872-4887.

[33] A. Suszka, Polish J of Chemistry, 1980, 54, 2289-2295.